ENDOR of the P2 centre in type-Ia diamonds

1993 J. Phys.: Condens. Matter 5 3019

(http://iopscience.iop.org/0953-8984/5/18/024)

J. Phys.: Condens. Matter 5 (1993) 3019–3026. Printed in the UK

ENDOR of the P2 centre in type-Ia diamonds

J A van Wyk and J H N Loubser

Department of Physics, University of the Witwatersrand, Wits 2050, Johannesburg, South Africa

Received 7 December 1992, in final form 9 February 1993

Abstract. The P2 centre was the first defect observed in diamond with electron spin resonance. Because of a very complicated ESR spectrum many years elapsed before the correct model was determined. Accurate spin Hamiltonian parameters have been determined from extensive ENDOR measurements at room temperature. These parameters are consistent with a model in which the defect consists of three nitrogens plus a vacancy. The observed ENDOR transitions do not follow the normal selection rules, and it will be explained how it can be predicted what frequencies will present in the ENDOR spectra.

1. Introduction

The P2 centre (Smith *et al* 1959a, Shcherbakova *et al* 1978, Loubser and Wright 1973 and van Wyk 1981) is frequently observed in type-Ia diamonds along with the P1 centre (Smith *et al* 1959b). It has been shown that this centre correlates with the N3 centre observed in optical spectroscopy (Davies *et al* 1977). Several models have been proposed for the defect (see references cited above), before preliminary ENDOR measurements by Loubser and Wright (1973) showed that the ENDOR spectra are consistent with one paramagnetic electron interacting with three nitrogen nuclei. Too few measurements, and a lack of computer facilities, however, hampered their determination of reliable parameters for the centre. Shcherbakova *et al* (1978) attempted to analyse its very complicated ESR spectra and published values for its spin Hamiltonian parameters. These parameters, as quoted, could not explain preliminary ENDOR results, neither could they reproduce the ESR spectra convincingly. An extensive ENDOR study was undertaken and parameters that describe both ESR and ENDOR results satisfactory were obtained. It will be shown that both the ESR and ENDOR results are consistent with the model shown in figure 1. In this model a vacancy is surrounded by three nitrogens and a carbon with a dangling bond. Note that the centre has trigonal symmetry around an axis joining the carbon adjacent to the vacancy (we will refer to this axis as the symmetry axis of the defect). ESR measurements (van Wyk 1982) showed that the paramagnetic electron is mainly localized on the carbon atom on the symmetry axis.

2. Experimental setup

A Varian large-sample access cavity and 100 kHz field modulation was used in conjunction with a Varian E-line spectrometer. Details about the method used to get samples in exactly the desired orientation, in the ESR cavity, and the technique used to observe the ENDOR signals, can be found in van Wyk *et al* (1992).

0953-8984/93/183019+08$07.50

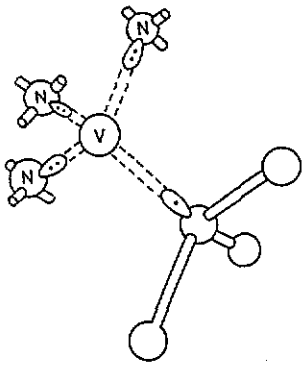

Figure 1. Model for the P2 centre. The unpaired electron is mainly localized on the carbon adjacent to the vacancy.

Normally the ESR spectra are recorded with the 100 kHz signal and reference voltage varying in phase with each other. However, it is known (Barklie and Guven 1981) that more intense ESR signals are observed for the P1 and P2 centres in many diamonds if the signal and reference are adjusted out of phase, and provided that the necessary adjustments are made to the microwave power level (moderately high) and the 100 kHz modulation amplitude (very low). The ENDOR signals were observed in this mode.

All measurements were taken at room temperature.

3. The spin Hamiltonian and energy levels

The model in figure 1 suggests that a single electron ($S = \frac{1}{2}$) is coupled to three identical nitrogen nuclei with $I = 1$. This gives rise to a system consisting of 54 energy levels, 27 in the $m_S = +\frac{1}{2}$ and 27 in the $m_S = -\frac{1}{2}$ manifold. ESR transitions occur from levels in one m_S manifold to the levels in the other manifold, whereas ENDOR transitions take place between levels within each manifold. Analysis of the ESR and ENDOR spectra amounts to assigning each absorption line to a specific transition. For the ESR spectra this is impossible, except for a few lines near the edges of the spectra, since the spectra consist of many overlapping lines. The ENDOR spectra, although not simple, consist of fewer and better-resolved lines, and absorption lines can be assigned to transitions with much greater confidence.

The spin Hamiltonian required is of the form

$$\mathcal{H} = \beta \boldsymbol{H} \boldsymbol{g} \boldsymbol{S} + \sum_{i=1}^{3} (\boldsymbol{S} \boldsymbol{A}_i \boldsymbol{I}_i - \beta_N \boldsymbol{H} g_{Ni} \boldsymbol{I}_i + \boldsymbol{I}_i \boldsymbol{P}_i \boldsymbol{I}_i)$$

where the symbols have their usual meaning. It is assumed that the principal values of the tensors involving nuclear spin are identical. The orientations of these principal axes, however, are symmetrically arranged with respect to the principal (trigonal) symmetry axis in figure 1.

The ESR spectrum and ENDOR frequencies can be calculated by solving the 54 x 54 secular equation resulting from the Hamiltonian above using standard computer routines. Since all the terms involving I are small, sufficiently accurate energies and ENDOR frequencies can however be calculated by solving the 6 x 6 secular equation of the spin

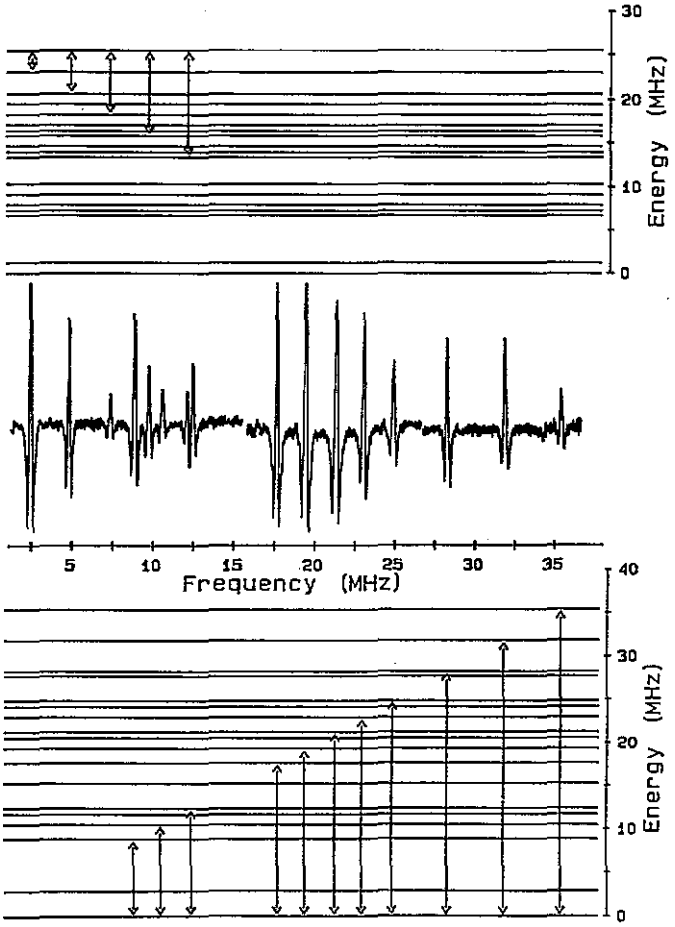

Figure 2. Typical example of the ENDOR spectrum of the P2 centre. The lowest ESR line is saturated (transition from lowermost to topmost level) with the magnetic field applied in a ⟨110⟩ direction. For this ESR line the magnetic field is perpendicular to both the main principal axes of g tensor and the hyperfine interaction.

Hamiltonian

$$\mathcal{H} = \beta \boldsymbol{H} \boldsymbol{g} \boldsymbol{S} + \boldsymbol{S} \boldsymbol{A}_i \boldsymbol{I}_i - \beta_N \boldsymbol{H} \boldsymbol{g}_{Ni} \boldsymbol{I}_i + \boldsymbol{I}_i \boldsymbol{P} \boldsymbol{I}_i$$

separately for each nitrogen involved in the centre, and then superimposing these to produce the energy level system appropriate for the centre. The energies, $E^+_{k\ell m}$, in the $m_S = +\frac{1}{2}$ manifold, for the composite system relative to the lowest level in this manifold, is given to a good approximation for the P2 centre by

$$E^+_{k\ell m} = (E^+_{1k} - E_{11})^+ + (E^+_{2\ell} - E^+_{21}) + (E^+_{3m} - E^+_{31})$$

where k, ℓ, m = 1, 2, or 3, and $E^+_{\alpha\beta}$ is the energy of level α in the $m_S = +\frac{1}{2}$ manifold for nitrogen β.

The ENDOR frequencies in this manifold for the composite system readily follow from this.

The energies and ENDOR frequencies for the $m_S = -\frac{1}{2}$ manifold can be calculated in the same manner.

It should perhaps be emphasized that the above approximate expression only holds because of the smallness of the hyperfine interaction.

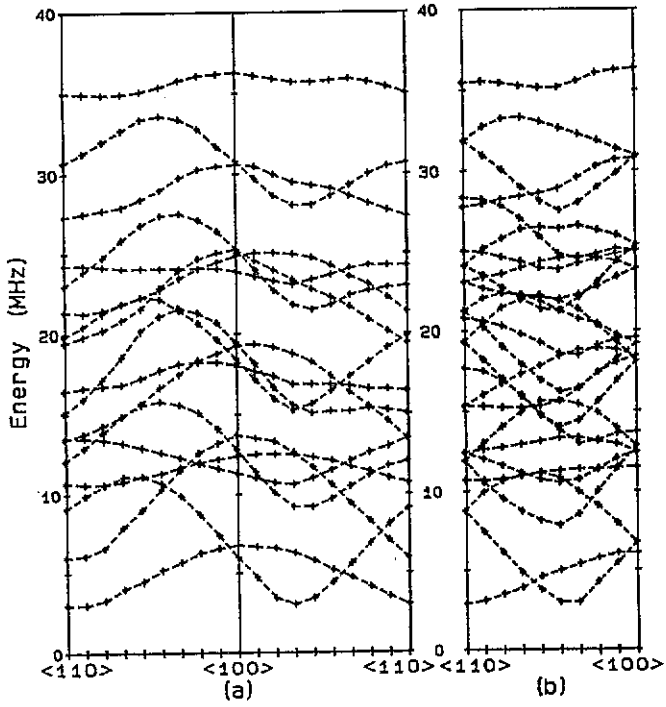

Figure 3. The angular dependence, in {110} planes, of the hyperfine energy levels, relative to the lowest energy level, of the 36 MHz manifold. The broken curves merely join the experimental points and have no other significance. (*a*) Planes containing the defect axis. (*b*) Planes that do not contain the defect axis.

4. The ENDOR spectra

A typical ENDOR spectrum is shown in figure 2. The magnetic field is applied in a ⟨110⟩ direction and adjusted so that the lowest ESR line is saturated. For this ESR line the magnetic field is at right angles to the symmetry axis of the defect.

Note that the ENDOR absorptions were not restricted to transitions to and from energy levels close to those involved in the ESR transition, as one may have expected from a $\Delta m_I = \pm 1$ selection rule.

ENDOR frequencies up to 36 MHz were observed in one m_S manifold, and up to 26 MHz in the other. These maximum frequencies correspond to $\Delta m_I = 2$ for all three nitrogens. The higher ENDOR frequencies in the 36 MHz manifold were observed only when the magnetic field was adjusted to transitions in the lower half of the ESR spectrum, whereas the higher frequencies in the 26 MHz manifold were only observed when the magnetic field was applied in the upper half of the ESR spectrum.

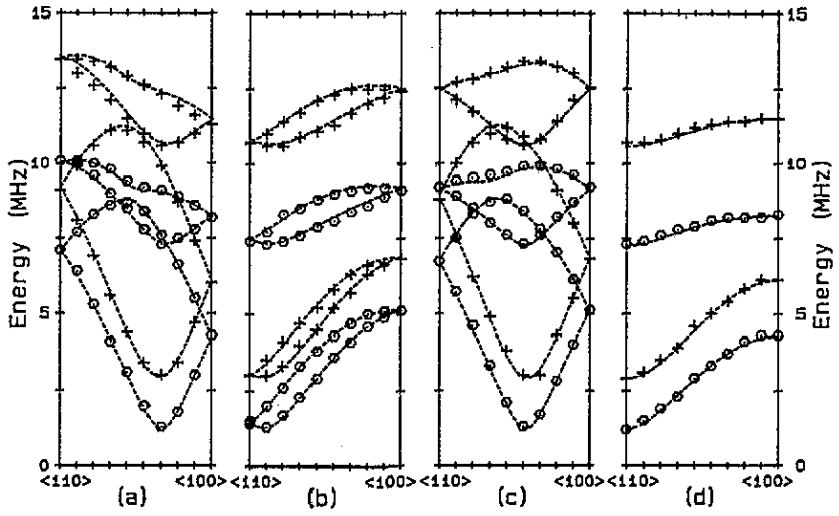

Figure 4. The angular dependence of single nitrogen ENDOR frequencies in the different {110} planes. The plus signs and hexagons are experimental values representing the 36 and 26 MHz manifolds, respectively. The curves were calculated using the values in table 1. (*a*) {110} plane containing symmetry axes of both the defect and hyperfine interactions. (*b*) {110} plane containing only the defect axis. (*c*) {110} plane containing the major hyperfine axis. (*d*) Neither the defect or the hyperfine axis is contained in this plane.

Although many ENDOR transitions were usually observed in one or the other manifold, some transitions were conspicuously absent when saturating certain ESR lines. An example is the transition between levels 1 and 2 (counting from the bottom) in figure 2. (The splitting between these levels is due to the hyperfine interaction with a nitrogen for which the magnetic field is at right angles to the main axis of the hyperfine interaction.) The transition is observed if the magnetic field is rotated only a few degrees from the ⟨110⟩ direction. The highest frequency is also not observed when the magnetic field is applied close to the main symmetry axis of the hyperfine interaction.

5. Angular dependence of the ENDOR frequencies

The angular dependences of the relative positions of the energy levels of the 36 MHz manifold as constructed from ENDOR measurements are shown in figure 3. Measurements with the magnetic field applied in both the lower and upper half of the ESR spectrum were used. A similar figure can be drawn for the 26 MHz manifold. It is a simple matter to extract from this figure, and the one for the 26 MHz manifold, the energy levels describing each nitrogen separately. These are represented in figure 4. The axial symmetry about an axis close to the axis joining the nitrogen and the vacancy is evident.

The hyperfine, quadrupole and nuclear Zeeman parameters in table 1 produced the best least-squares fit to the data in figure 4. The g tensor, determined from ESR measurements, is axially symmetric around the defect axis, whereas the hyperfine tensors are axially symmetric about axes close to the ⟨111⟩ axes joining the vacancy and a nitrogen. These parameters and axes were used to calculate the full curves in figure 4. It is perhaps worth noting that any change in the accepted value of g_N, namely −0.404, leads to an increase in

Table 1. Spin Hamiltonian parameters for the P2 centre.

		Loubser and Wright (1973)	Shcherbakova *et al* (1978)	This work
g tensor	$g_{\parallel}$	—	2.0025	2.0023(2)
	$g_{\perp}$	—	2.0031	2.0032(2)
	$\theta(^{\circ})^{\dagger}$	—	35.26	35.26
A tensor (MHz)	A_1	10.1	9.1	7.4(1)
	A_2	10.1	8.8	7.4(1)
	A_3	11.0	10.4	11.2(1)
	$\theta(^{\circ})^{\dagger}$	35.26	139	158(1)
P tensor (MHz)	$P_{\parallel}$	−1.0	+3.1	−4.8(1)
	γ	0.0	0.0	0.0
	$\theta(^{\circ})^{\dagger}$	35.26	139	145(2)
	g_N	0.404	0.404	0.404

† θ is measured from a ⟨110⟩ axis.

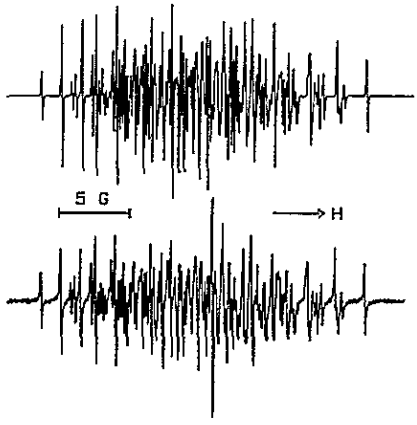

Figure 5. The calculated (top) and experimental (bottom) ESR spectra with the magnetic field applied along a ⟨100⟩ direction.

the sum of the squares of the residuals, showing that there can be no doubt that the nuclei involved must be nitrogen.

6. ESR and ENDOR transition probabilities

The ESR transition probabilities can be calculated once the secular equation is solved. For this purpose the full 54 x 54 had to be used. As is to be expected, many transitions are possible. The calculated and experimental spectra with the magnetic field applied along a ⟨100⟩ axis are shown in figure 5.

Newton put forward a proposal that explains the observed ENDOR transitions for the N3 centre in type-Ib diamonds (van Wyk *et al* 1992). This proposal also correctly predicts which ENDOR transitions are expected for the P2 centre. Basically, an ENDOR transition between levels i and k in one of the manifolds will be observed if there is an ESR transition

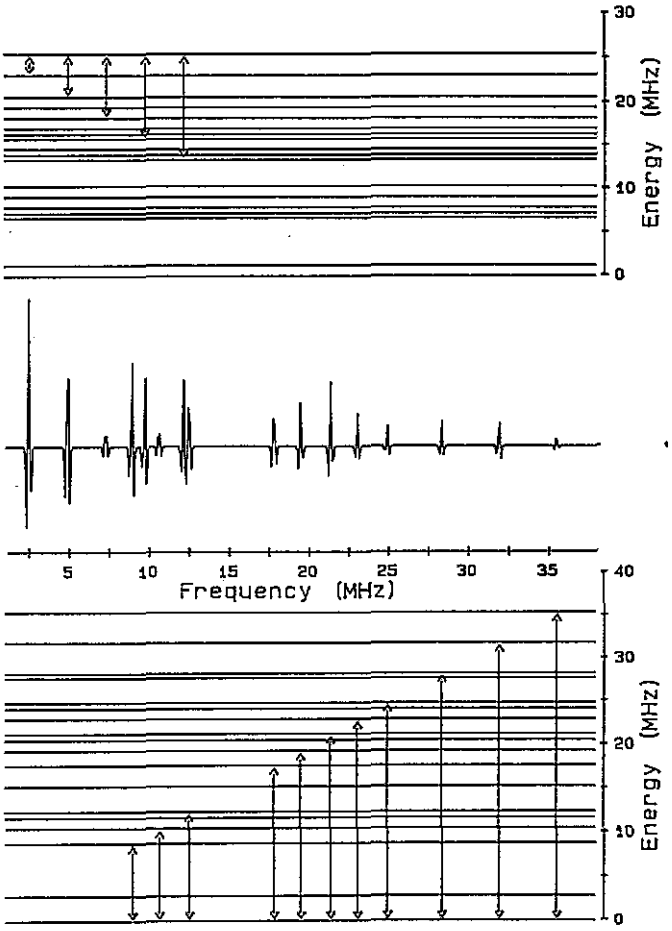

Figure 6. Calculated intensities of the ESR transitions involving the uppermost and lowermost energy levels with the magnetic field applied along the ⟨110⟩ at right angles to the symmetry axis of the defect. The intensities (not shown) of the ENDOR transitions (indicated by the arrows) shown should depend on the intensities of the ESR transitions. The intensities of the ESR transitions in this diagram must be compared with the intensities of the experimental ENDOR lines in figure 2.

that short circuits (large transition probability) levels k and j when the ESR transition $i \rightarrow j$ is saturated. This is demonstrated in figure 6, where it is assumed that the ESR transition between the lowermost and uppermost energy levels is saturated. The relative ESR transition probabilities involving the uppermost and lowermost energy levels are plotted against the ENDOR frequencies that will result when these transitions short two hyperfine levels. The probabilities for transitions not shown in figure 6 are too low to show up with the scale used in figure 6. This must be compared with the ENDOR spectrum in figure 2. The agreement is almost too good to be true.

7. Discussion

The main reason why Shcherbakova's parameters fail to describe the ENDOR and ESR measurements satisfactory seems to lie with the quoted value of the quadrupole parameter P. Changing only the sign of P, however, still left us with glaring differences between the experimental and calculated ESR and ENDOR spectra. The new parameters correctly describe the experimental spectra.

The ENDOR results are clearly consistent with model of the P2 centre as shown in figure 1.

The hyperfine tensor can be used in the usual manner (Smith *et al* 1959a, b), to calculate the p/s ratio of the electron ψ_{2p} and ψ_{2s} densities in the nitrogen hybrid orbital interacting with the paramagnetic electron. The value obtained is 4.75, which is slightly larger than the corresponding value of 3.85 for the P1 centre. This shows that each nitrogen in the P2 centre relaxed somewhat more into the plane of the carbons it is bonded to, than is the case for the P1 centre.

The magnitude of the quadrupole term ($P_{\parallel}$) is significantly larger for the P2 centre than for most other nitrogen centres observed in diamond so far (see, for example, Cox *et al* 1992). An important difference between the P2 and the other defects is the presence of the vacancy. The significance of this will be discussed in more detail in a future paper.

Acknowledgments

The authors would like to thank the management of the Diamond Research Laboratory of the De Beers Industrial Division for providing the diamonds required in this work. We would also like to thank Diamond Research Laboratories and the Condensed Matter Research Unit for their financial support.

References

Barklie R C and Guven J 1981 *J. Phys. C: Solid State Phys.* **14** 3621–31
Cox M E, Newton M E and Baker J M 1992 *J. Phys.: Condens. Matter* **4** 8119–30
Davies G, Welbourn C M and Loubser J H N 1978 *Diamond Research* pp 23–30
Loubser J H N and Wright A C J 1973 *Diamond Research* pp 16–20
Shcherbakova M Ya, Nadolinnyi V A and Sobolev E V 1978 *Zh. Strukt. Khim.* **19** 305–14
Smith W V, Gelles I L and Sorokin P P 1959a *Phys. Rev. Lett.* **2** 39–40
Smith W V, Sorokin P P, Gelles I L and Lasher G J 1959b *Phys. Rev.* **115** 1546–52
van Wyk J A 1982 *J. Phys. C: Solid State Phys.* **15** L981–3
van Wyk J A, Loubser J H N, Newton M E and Baker J M 1992 *J. Phys.: Condens. Matter* **4** 2651–62